ADVANCED FUNCTIONAL MATERIALS
www.afm-journal.de

Energy-Dissipative Matrices Enable Synergistic Toughening in Fiber Reinforced Soft Composites

*Yiwan Huang, Daniel R. King, Tao Lin Sun, Takayuki Nonoyama, Takayuki Kurokawa, Tasuku Nakajima, and Jian Ping Gong**

Tough hydrogels have shown strong potential as structural biomaterials. These hydrogels alone, however, possess limited mechanical properties (such as low modulus) when compared to some load-bearing tissues, e.g., ligaments and tendons. Developing both strong and tough soft materials is still a challenge. To overcome this obstacle, a new material design strategy has been recently introduced by combining tough hydrogels with woven fiber fabric to create fiber reinforced soft composites (FRSCs). The new FRSCs exhibit extremely high toughness and tensile properties, far superior to those of the neat components, indicating a synergistic effect. Here, focus is on understanding the role of energy dissipation of the soft matrix in the synergistic toughening of FRSCs. By selecting a range of soft matrix materials, from tough hydrogels to weak hydrogels and even a commercially available elastomer, the toughness of the matrix is determined to play a critical role in achieving extremely tough FRSCs. This work provides a good guide toward the universal design of soft composites with extraordinary fracture resistance capacity.

1. Introduction

In general, producing materials that possess both high strength and toughness is extremely difficult and has rarely been realized.[1–3] This is because these two properties are often contradictory.[2] Nature has overcome this conflict and developed materials exhibiting both excellent load-bearing capacity and fracture resistance, as can be observed from both hard tissues[3–7] (e.g., nacre and bone) and soft tissues (e.g., ligament and tendon),[8–10] by combining rigid, brittle components (either inorganic or organic) and soft, organic components into composite materials. Most of these natural materials have highly complex hierarchical architectures existing over multiple length scales, which results in composite properties that far exceed what could be expected from a simple combination of the individual components.[3] Many researchers have attempted to mimic the unique natural structures of tough, hard hybrid materials, but only a few studies have achieved remarkable success comparable to that of nature.[11–14] For example, a bioinspired alumina hybrid material with specific strength and toughness comparable to aluminum alloys was synthesized by combining a hard yet brittle ceramic with relatively soft poly(methyl methacrylate), where nacre-like multiple toughening mechanisms at multiple scales resulted in exceptional fracture resistance.[12]

As a vital class of soft materials, tough hydrogels have shown strong potential as structural biomaterials.[15–20] These hydrogels alone, however, still possess limited mechanical properties (low modulus) when compared to some load-bearing tissues, e.g., ligaments and tendons. To reproduce the exceptional strength and toughness seen in soft load-bearing tissues, one strategy is to combine an energy-dissipative tough hydrogel with rigid yet flexible fibers to create a composite, similar to fibrous tissues.[21–23] In this composite concept, the rigid fiber-based component increases the specific strength while the gel matrix dissipates energy. Based on this concept, some attempts have been made to fabricate fiber reinforced hydrogel composites.[24–29] Utilizing this technique, researchers have been able to increase and tune the stiffness and toughness achievable with hydrogel-based systems. However, developing soft composites with synergistically improved mechanical properties, such as those seen in hard bioinspired composites, is still a challenge.

Recently, our group has developed a new class of tough hydrogels, polyampholyte (PA) gels (fracture energy, $T = 3000$ J m^{-2}), based on multiple ionic bonds acting as reversible sacrificial bonds in the gel network.[18,30] Interestingly, PA gels also demonstrate unique interfacial bonding to charged surfaces, either positive or negative, due to the self-adjustable Coulombic interaction of the dynamic ionic bonds of the PA.[31] The PA gels are synthesized from radical polymerization of oppositely

Y. Huang
Graduate School of Life Science
Hokkaido University
Sapporo 001-0021, Japan
Dr. D. R. King, Dr. T. L. Sun, Dr. T. Nonoyama, Dr. T. Kurokawa, Dr. T. Nakajima, Prof. J. P. Gong
Faculty of Advanced Life Science
Hokkaido University
Sapporo 001-0021, Japan
E-mail: gong@sci.hokudai.ac.jp
Dr. D. R. King, Dr. T. L. Sun, Dr. T. Nonoyama, Dr. T. Kurokawa, Dr. T. Nakajima, Prof. J. P. Gong
Global Station for Soft Matter
Global Institution for Collaborative Research and Education
Hokkaido University
Sapporo 001-0021, Japan

DOI: 10.1002/adfm.201605350

charged monomers. In contrast to traditional hydrogels that swell in water, the as-prepared PA gels undergo a deswelling process in water by dialysis of small counterions, which favors the enhancement of both gel toughness and surface adhesion to charged surfaces.[32,33] The combined superior properties of PA gels provide us with the raw materials necessary to realize our target of achieving fiber reinforced soft composites (FRSCs) with both superior strength and toughness. To demonstrate our concept, we have recently introduced a new material design strategy by combining soft PA gels with woven glass fiber fabric (GF) to fabricate PA-GF hydrogel composites.[34] The glass fiber fabric was chosen because its surface has negative charges in water, and can form good adhesion with PA gels, improving interfacial bonding.[31,35–37] In that study, the new composites using a PA hydrogel matrix, P(NaSS-*co*-DMAEA-Q) (copolymerized from sodium *p*-styrenesulfonate (NaSS) and dimethylaminoethylacrylate quaternized ammonium (DMAEA-Q) (Figure S1, Supporting Information)), exhibited extremely high effective toughness (250 kJ m^{-2}), high tearing strength (≈65 N mm^{-1}), and high tensile modulus (606 MPa). These properties are far superior to those of either the PA hydrogel or glass fabric, indicating a synergistic effect. As the hydrogel composites contain water (≈38 vol% water) and are likely biocompatible (encompassed by ≈44 vol% biocompatible soft polymers) (Table S1, Supporting Information),[18] they exhibit some structural similarities with load-bearing natural tissues. We believe that these impressive results provide a simple route to develop extremely tough and biocompatible soft materials.

We consider that the highly energy-dissipative gel matrix and its unique interfacial bonding with glass fabric are the two critical factors for achieving the synergistic effect in toughness of the composites. In this work, we focus on understanding the role of energy dissipation of the matrix in FRSCs. To isolate this variable, we select a specific fabric type and geometry, where the glass fibers are woven in a plain weave (**Figure 1**) and the strength of the fibers is relatively high so that the failure of the composites always occurs due to pull-out of the fibers, by fracture either at the fiber-matrix interface or in the bulk of matrix. We use the PA hydrogel, P(NaSS-*co*-DMAEA-Q), as the matrix, and perform experiments to alter the matrix toughness to study its effect on the toughness of the soft composites.[18,30] First, we varied the effective PA gel toughness by changing the tearing velocity, taking the advantage of the strong viscoelasticity of PA gels due to dynamic Coulombic interactions between oppositely charged ionic groups.[18,38] Second, we tuned the PA gel toughness using saline solutions, because the ionic bonds in the PA gel are sensitive to ionic strength.[18,38] Finally, to expand our understanding of this system and attempt to understand the universality of the relationship between matrix toughness and composite toughness, we further selected a series of weak polyacrylamide hydrogels and a commercially available polydimethylsiloxane elastomer as soft matrices. Through these experiments, we have discovered that for samples exhibiting the fiber pull-out mechanism, a universal scaling law exists, relating the toughness of the matrix to the soft composite. This discovery on the importance of matrix toughness in FRSC systems provides a path toward the design of extremely tough composites from various soft materials such as hydrogels and elastomers.

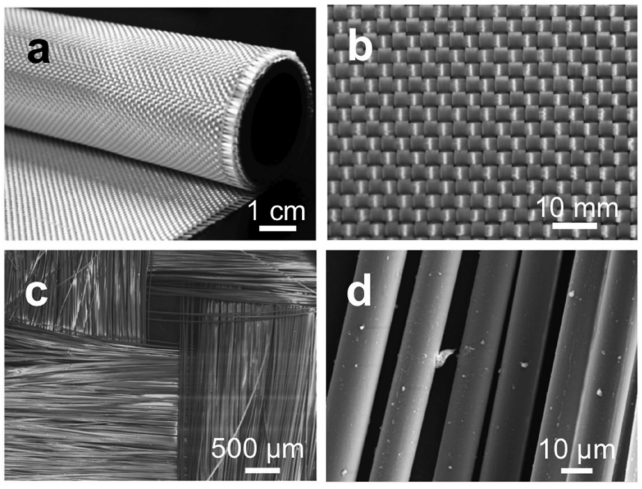

Figure 1. Structure of the neat woven glass fiber fabric (GF). Macroscopic images of a) the commercially available glass fiber fabric and b) the plain weave structure. SEM images of c) a single weave of the fiber fabric and d) individual glass fibers. The effective Young's modulus and ultimate tensile strength (in the direction of fiber alignment) of the fabric are $E = 5.49 \pm 0.04$ GPa and $\sigma_u = 242.26 \pm 10.50$ MPa, respectively.

2. Results

2.1. Morphology of PA-GF Hydrogel Composites

To create a good composite, it is important to ensure that a strong interface exists between the matrix and the reinforcing material. Even at the high molar concentration (C_m = 2.5 M) used here, the PA precursor solution is highly fluid. Furthermore, the glass fibers are strongly hydrophilic. This combination ensures excellent wetting and penetration of the precursor monomer solution into the fiber bundles (Figure S2, Supporting Information). After the radical polymerization, the surface is covered, and the interstitial space within the fiber bundles is filled with the PA gel matrix to form a continuous structure (**Figure 2**). The presence of a large number of individual fibers provides sufficient surface area for forming strong interfacial bonding between the hydrogel matrix and the fabric.

2.2. Fracture Behavior of PA-GF Hydrogel Composites

Trouser tearing tests are used to understand the fracture process of the composites. The images of the fracture behavior of the composites during the test are shown in **Figure 3**a–c, and the representative tearing force versus displacement curves for the neat PA gel, neat fabric, and PA-GF hydrogel composite are shown in Figure 3d. We first analyze the images of the fracture process. Before testing, a 20 mm initial notch is placed nominally at the center of the samples (width, w = 45 mm, total length, L = 47.5 mm) using a rotary cutter (Figure 3a). One "leg" of the sample is attached to the base of the tensile tester, and the other leg is attached to the crosshead (Figure 3b(1)), which is displaced at 50 mm min^{-1}. During testing, the notch

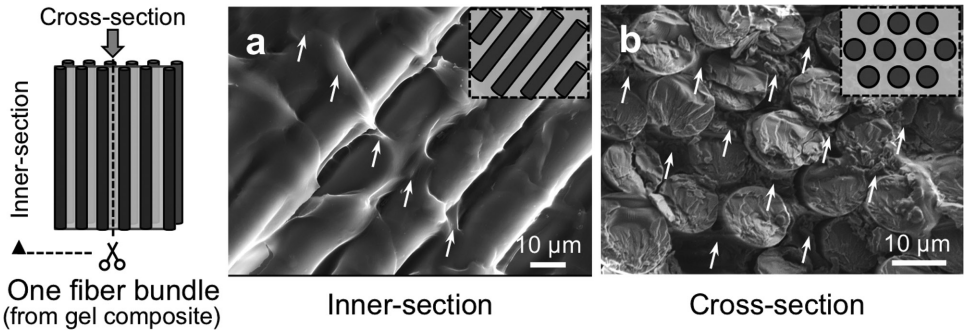

Figure 2. SEM images inside a fiber bundle of the PA-GF hydrogel composite after polymerization. To check the existence of hydrogel matrix inside the fiber bundles, one fiber bundle from the hydrogel composite was cut in two different orientations. Images were taken a) along the length of the fibers and b) of the cross-section of the fibers. The light gray color in the inserted schematics indicates the hydrogel matrix. The polymer matrix (indicated by white arrows) filled the interstitial space in the fiber bundles and connected the neighboring fibers.

in the composite sample does not immediately propagate, but is largely stretched and blunted at the tip (Figure 3b(2)), similar to the crack blunting observed in neat, tough PA gels as well as fibrous animal tissues.[9,38] The high load in the region around the notch results in a significant deformation of the bulk sample (highlighted region in Figure 3b(2)–(4)), which effectively diminishes the stress concentration at the notch and should significantly contribute to the energy dissipation. Before the fracture process begins, the sample reaches a maximum stretch (Figure 3b(3)), corresponding to the highest force of fracture resistance (Figure 3d). Additional displacement results in gel matrix fracture and fiber pull-out of the deformed bulk region. The composite sample continues to stretch as the transverse fiber bundles are slowly pulled out of the weave (Figure 3b(4) until the sample completely fails. During tearing, as more transverse fiber bundles are pulled out of the weave, the remaining bulk becomes smaller, resulting in the gradually reduced tearing force. After failure, we see evidence of the bulk energy-dissipative processes in Figure 3c. In the left sample fragment, fractured gel matrix in the fabric is visible, and the

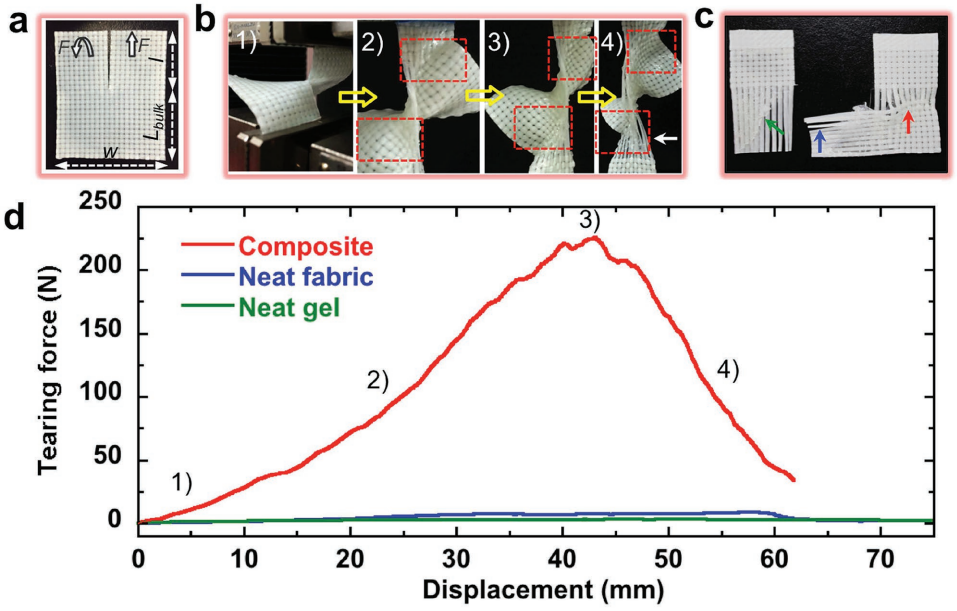

Figure 3. High tear resistance of PA-GF hydrogel composites in comparison to the neat components. a) A representative hydrogel composite in a trouser tearing test geometry with a sample width $w = 45$ mm, a bulk length $L_{bulk} = 27.5$ mm, and an initial leg length $l = 20$ mm for the tearing test. b) The sequence of events of a tearing test where a representative notched composite is strained. The notch in the hydrogel composite undergoes large strain prior to propagation under tearing loading. The red dashed frame in subfigure-(2–4) indicates the significant deformation to the sample bulk. The white arrow in subfigure-(4) indicates pull-out of the fiber bundles. c) The left sample fragment shows fractured gel matrix (green arrow). The right sample fragment possesses the fibers which were pulled out during tearing (blue arrow), and shows evidence of residual deformation formed prior to the fibers pulling out (red arrow). d) Tearing force versus displacement curves for the H_2O-equilibrated neat polyampholyte hydrogel, neat fabric, and H_2O-equilibrated PA-GF hydrogel composite. The sample width of both neat fabric and hydrogel composite is $w = 45$ mm. The tearing velocity is 50 mm min^{-1}. The tearing behavior of the numbered positions on the curve of the hydrogel composite can be visually understood from the sequence of events shown in (b).

right sample fragment shows the fibers that are pulled out of the fabric weave, as well as the presence of residual deformation around the original notch location (Figure 3c). It should be noted that during fracture this deformation is present around the entire crack area, yet evidence is only visible on one fragment because fiber pull-out occurs on the opposing side.

As shown in Figure 3d, the hydrogel composite achieves extremely high tearing force in comparison to that of either the neat PA gel or neat fabric. The maximum tearing strength value (calculated from the tearing force divided by the fabric thickness) for the 45 mm width composite sample reaches ≈380 N mm^{-1}, which is several orders of magnitude greater than both individual neat materials (≈1.90 N mm^{-1} for neat PA gel and ≈14.70 N mm^{-1} for neat fabric). The exceptionally high tear resistance of the PA-GF composite far exceeds what could be expected from the simple additive combination of its components, demonstrating a strong synergistic effect. To achieve this effect, the fibers must be completely coated with the gel to maximize energy dissipation. We find that the tearing energy of the composite increases with increasing composite thickness and becomes saturated at a constant value when the as-prepared composite thickness is approximately three times the fabric thickness (Figure S3, Supporting Information). This indicates that the soft composite thickness should be above a critical value (three times of the fabric thickness) to achieve good mechanical performance. Therefore, all of the following studies are performed with a total sample thickness at least three times the fabric thickness.

2.3. The Role of Matrix Toughness in PA-GF Hydrogel Composites

Based on the above observations, for the neat fabric, only the frictional force between the fiber bundles during fiber pull-out is responsible for the fracture resistance and energy dissipation during tearing, leading to very limited tearing toughness. In comparison, when integrated with the tough PA gel, the pull-out of the fiber bundles requires matrix deformation and fracture, as revealed by the scanning electron microscope (SEM) images (Figure 2), resulting in a composite with exceptionally high tear resistance. This leads us to investigate the importance of the matrix in the toughening of woven fabric composites.

To verify the importance of matrix toughness, we first investigate the tearing velocity-dependence of PA-GF hydrogel composites (**Figure 4**). According to previous studies,[18,38] the PA gels exhibit viscoelasticity, leading to a strong velocity-dependence in mechanical properties, e.g., tensile and tearing

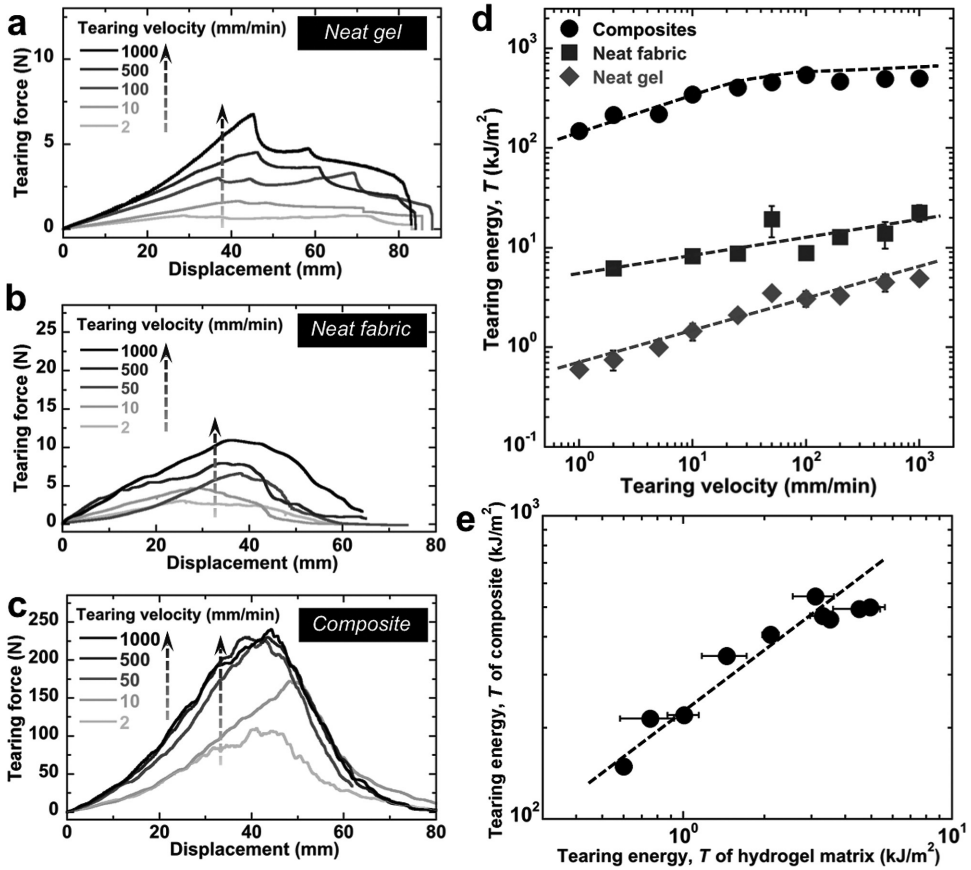

Figure 4. Tearing velocity dependent behaviors of the H_2O-equilibrated PA-GF hydrogel composite. Tearing force versus displacement curves for a) the neat gel, b) neat fabric, and c) the hydrogel composites at different tearing velocities. The sample width of both the neat fabric and composite is w = 45 mm. d) Tearing energy, T, of the neat gel, neat fabric, and hydrogel composite versus tearing velocity. e) Tearing energy of the composite hydrogels versus the tearing energy of the hydrogel matrix, based on the above data. Dashed lines in (d) and (e) are manually drawn as visual guides.

properties (Figure 4a and Figure S4, Supporting Information). The tearing energy, T, of the neat PA gels increases accordingly with increasing tearing velocity (Figure 4d).[38] The neat fabric also shows a slightly increased tearing force in the tearing velocity range from 2 to 1000 mm min^{-1} (Figure 4b), due to its weakly viscoplastic deformation. When combined with woven glass fiber fabric, the PA-GF hydrogel composites achieve greatly increased tearing properties and also show a velocity-dependent tearing behavior (Figure 4c,d), similar to that of the neat PA hydrogels. However, when the tearing velocity is sufficiently high (v > 50 mm min^{-1}), the tearing force and tearing energy of the composites become relatively insensitive to the tearing velocity, differing slightly from those of the neat hydrogels.

When we plot the T values of the composites versus the T values of the matrix at different tearing velocities, as shown in Figure 4e, we find that the composite toughness correlates with the matrix toughness, roughly, by a power-law relation. This result suggests the importance of the matrix toughness in achieving extremely tough hydrogel composites.

As discussed in a previous study,[18] the ionic bonds in PA gels can be destroyed in aqueous solutions with high ionic strength, resulting in decreased toughness of the hydrogel. Therefore, we further tune the toughness of the PA gel by equilibrating the samples in sodium chloride (NaCl) solutions with varied ionic strength. As indicated in Figures S5 and S6 (Supporting Information), for a fixed tensile or tearing velocity, the modulus, fracture stress, and tearing force of the PA gel decreases substantially in the NaCl solutions, indicating that a significant number of ionic interactions are destroyed. In accordance with this result, the tearing force of the PA-GF composite also decreases accordingly (Figure S7, Supporting Information), indicating again, that the composite toughness is correlated to that of hydrogel matrix.

The tearing energy, T, of the PA gel and the composite is plotted against the square root of the NaCl concentration, $C_{NaCl}^{1/2}$ in **Figure 5**a. According to the Debye–Huckel theory,[39] the Coulombic interactions decrease with increasing ionic strength, C_{NaCl}, of the bath solution with $C_{NaCl}^{1/2}$. It can be found that with increasing $C_{NaCl}^{1/2}$, the tearing energy of the composites decreases, due to the weakened toughness of the PA gel matrix. The swelling ratio (in sample thickness) of the PA gel and PA-GF hydrogel composites versus the ionic strength, $C_{NaCl}^{1/2}$, is shown in Figure S8 (Supporting Information). When $C_{NaCl}^{1/2}$ is very small (e.g., C_{NaCl} = 0.01 and 0.05 M), the geometry of the samples is almost the same as that of the H_2O-equilibrated samples. However, the tearing energy of both the neat gel and the composite dramatically decreases, further confirming the correlation between the hydrogel matrix toughness and the hydrogel composite toughness.

The fracture images of the composite samples after tearing show evidence of the importance of matrix toughness. As ionic strength, C_{NaCl}, increases, the bulk sample deformation decreases (less residual deformation is evident) and the amount of gel present on the pulled-out fibers increases (**Figure 6**). Two observations can be drawn from these results. First, as matrix toughness decreases, fracture continues to occur in the matrix, rather than simply at the interface. This leads us to the conclusion that even in the high ionic strength samples, there is sufficient interfacial bonding to distribute stress to the matrix. Furthermore, these results indicate that the fracture of the weakened PA gel matrix appears to occur more easily during tearing, resulting in decreased tearing resistance capacity.

To further explore the relationship between the matrix toughness and the composite toughness, similar to the analysis of tearing velocity-dependence data, we also plot T of the hydrogel composites versus T of the hydrogel matrix for different saline solutions in Figure 5b. Again, we see a good power-law correlation between composite toughness and matrix toughness.

The ionic strength effect on the toughness of the neat PA gel and its composite also helps us understand the behaviors of the as-prepared samples. As presented in Figures S9–S11 (Supporting Information), the as-prepared PA-GF hydrogel composite before dialysis in water exhibits relatively poor tearing properties, which is due to the strong screening effect of the high ionic strength of the counterions in the as-prepared PA gel matrix (ionic strength C_{NaCl} = 2.5 M, T = 211 J m^{-2} at a tearing velocity 50 mm min^{-1}). After dialysis, the counterions are removed from the composite, and the PA gel matrix becomes very tough (T = 3510 J m^{-2}) due to the formation of

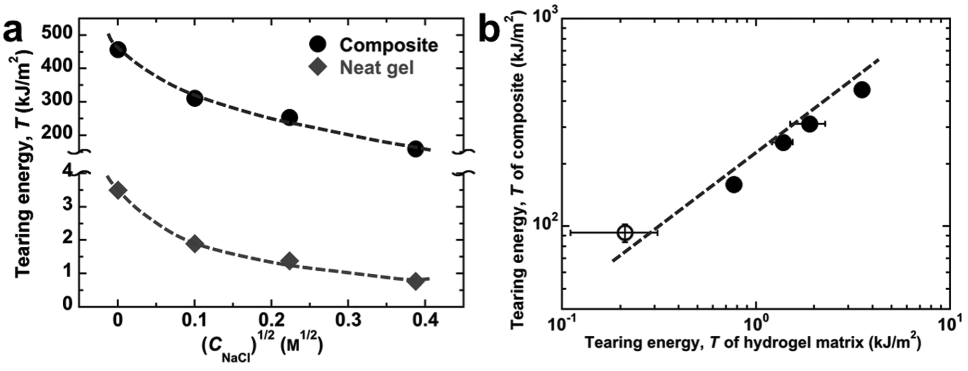

Figure 5. Tearing behaviors of the H_2O-equilibrated PA hydrogel and PA-GF gel composites after achieving their equilibrium in NaCl solutions with different concentrations. a) Tearing energy, T, versus ionic strength, $C_{NaCl}^{1/2}$, for the PA gels and composites. The sample width of the composites is w = 45 mm, and the tearing velocity is 50 mm min^{-1}. b) Tearing energy of the hydrogel matrix versus tearing energy of the composite hydrogels for samples in different NaCl concentrations. The open circle represents the result of the as-prepared sample (C_{NaCl} = 2.5 M) (see details in Figures S9–S11 in the Supporting Information). Dashed lines are manually drawn as visual guides.

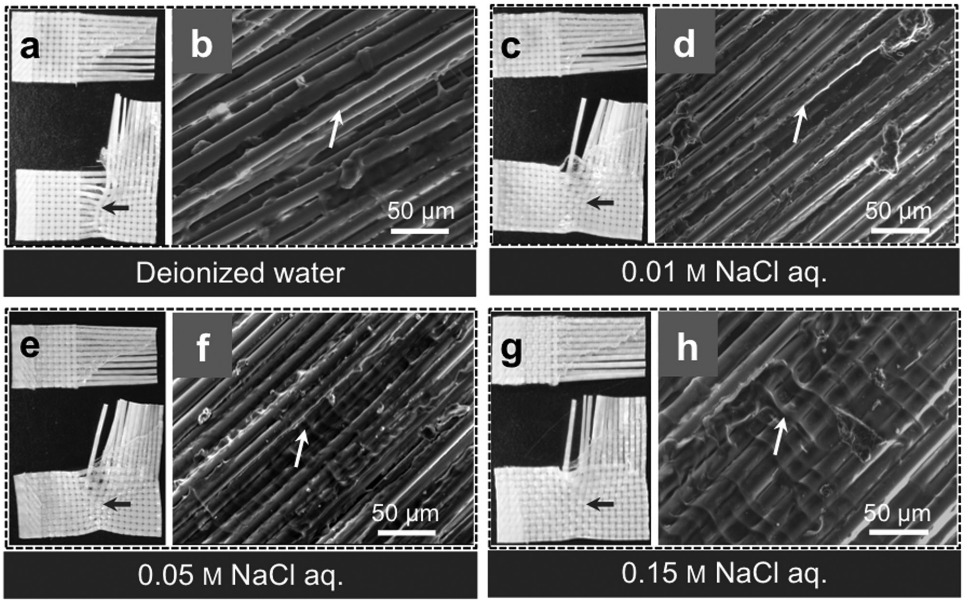

Figure 6. Macroscopic and microscopic images of the composite samples after fracture. The dark gray arrow in each image indicates the area where residual deformation is seen. As ionic strength increases, less residual deformation is present. The white arrow indicates the hydrogel matrix adhered on the fibers after the tearing test. a,b) The H_2O-equilibrated PA-GF hydrogel composite. c–h) The PA-GF gel composites equilibrated in different saline solutions.

ionic interactions in the gel network, resulting in the greatly improved tearing toughness for the H_2O-equilibrated hydrogel composite. The as-prepared result also falls on the same master line in Figure 5b.

Based on the above results, we can conclude that the energy-dissipative PA hydrogel matrix is critical for achieving extremely tough PA-GF hydrogel composites. The fracture behavior of the composite indicates that the energy dissipation of the bulk surrounding the crack tip dominantly contributes to the high tearing energy. This is analogous to de Gennes' trumpet model proposed to explain the fracture resistance of a viscoelastic rubber.[40] Such mechanism also likely occurs to strengthen the PA gel-fiber interface of the composite, as suggested by researches for gel-nanoparticle interface adhesion.[32] These processes enable large energy dissipation during composite fracture.

2.4. Universality of the Scaling Law

Interestingly, we discovered that the composite toughness follows a power-law relationship with the hydrogel matrix toughness over a relatively wide scale (Figures 4 and 5). To understand the universality of the power-law relationship between the matrix toughness and the composite toughness at the given fiber pull-out mechanism, we further select a series of weak polyacrylamide (PAAm) hydrogels and a commercially available elastomer based on polydimethylsiloxane (PDMS) as soft matrices, in the following discussion.

Chemically cross-linked PAAm hydrogels represent a common class of single network hydrogels that have high water content. Due to a lack of sacrificial bonds to dissipate energy, PAAm hydrogels are elastic and therefore mechanically weak. The fracture toughness of the PAAm hydrogels is proportional to the polymer chain length between the cross-linking points and the areal chain density across the fracture surface, according to the Lake–Thomas theory.[41] While usually interfacial chemistry is required to enable PAAm to adhere well to glass surfaces,[32,33] the in situ polymerization process, in combination with the large area of contact with the fibers, enables sufficient interfacial bonding. We adopt the as-prepared PAAm hydrogels with variable chemical cross-linker concentration to study the effect of a weak matrix on the composite. As predicted by rubber elasticity and the Lake–Thomas theory, increasing the chemical cross-linker percentage results in increased modulus and decreased toughness of the PAAm hydrogel, respectively (Figure S12, Supporting Information). Both samples show poor toughness compared to the PA gels. The tearing test results (Figure S13a,b, Supporting Information) show that for both PAAm composites there is no significant improvement in tearing energy compared to the neat fabric. After tearing, PAAm composites show no sign of residual deformation, unlike the H_2O-equilibrated PA composites, further proving the low energy dissipation capacities (Figure S13c, Supporting Information) of these materials.

The toughness of the chemically cross-linked PAAm hydrogels should increase with increasing polymer chain areal density for a fixed partial chain length, according to the Lake–Thomas theory.[41] We further reduce the water content of the PAAm hydrogel by equilibrating the samples in poly(ethylene glycol) (PEG) solution to increase the toughness of the PAAm hydrogel (Figure S14, Supporting Information). In a similar manner, a deswollen PAAm-GF composite is obtained. A slight increase in the toughness of the PAAm hydrogel also brings about a slight increase of the toughness of the composite (Figure S15, Supporting Information).

Moving beyond hydrogel systems, we also selected a commercially available PDMS elastomer, SILPOT 184, as a soft matrix, which does not contain water. The neat elastomer has a relatively high modulus (≈0.88 MPa), fracture stress (≈6.75 MPa), and a moderate tearing energy (≈960 J m^{-2}) compared with hydrogel materials (Figure S16, Supporting Information). The elastomer is able to achieve sufficient interfacial interactions between the matrix and the glass due to strong van der Waals interactions.[42,43] By combining PDMS with the woven glass fabric, the PDMS-GF composite demonstrates a relatively high tearing force compared to the neat fabric (Figure S17a, Supporting Information). When comparing the tearing energy, T, values (Figure S17b, Supporting Information), the PDMS-GF composite shows a moderate T value between that of the as-prepared PA-GF composite and that of the H_2O-equilibrated PA-GF composite. The fracture images of the samples after tearing (Figure S17c,d, Supporting Information) show that the composite also experienced a fiber pull-out failure behavior, and a large amount of polymer is seen on the bundle, similar to the as-prepared PA-GF hydrogel composite (Figure S11, Supporting Information). This result agrees with the results of the fiber-reinforced hydrogel composites, and further indicates the existence of a strong relationship between matrix toughness and the resulting composites toughness.

3. Discussion

The mechanical properties of the woven glass fabric composites fabricated in this work are summarized in Table S2 (Supporting Information). To verify the universality of the correlation between the soft matrix toughness and the composite toughness, we plot the tearing energy of the composites, T_c, versus the tearing energy of the soft matrices, T_m, with log–log axes, from all the tearing energy data (**Figure 7**). This plot clearly demonstrates that the composite toughness follows an empirical power-law equation, $T_c = 220\ T_m^{0.64}$, over two orders of magnitude of the soft matrix toughness, for different chemical structures of the matrix phase. In comparison, we also plot the tearing energy of the composites versus other mechanical properties of their matrices, including fracture stress, Young's modulus, and fracture strain (Figure S18, Supporting Information). These variables lack any clear trend, reinforcing our hypothesis that the toughness of the matrix is the key parameter determining the toughness of FRSCs.

The observed power-law equation between the matrix and the composite indicates that the fracture resistance of the composite is related to the matrix bulk energy dissipation, in the limit of the given fiber pull-out mechanism. The relatively strong interfacial bonding between the matrix and fibers effectively transfers the load to the matrix phase. This allows the load to be widely distributed and results in energy dissipation by the matrix phase. Furthermore, even for a relatively poor interfacial bonding systems, the intercalation of the matrix with the fiber bundle makes the bulk matrix deform and fracture during the fiber pull-out process and therefore acts as the dominant energy dissipation mechanism for the composite.

As clearly shown in Figure 7, when the matrix toughness is very low, the composite toughness approaches the additive law

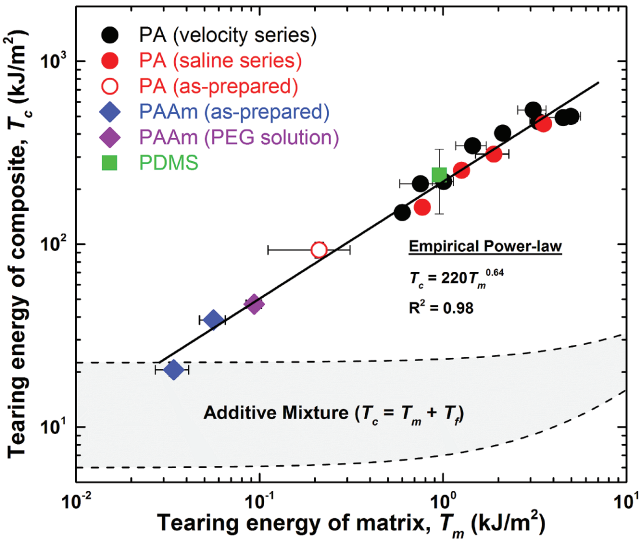

Figure 7. Tearing energy of the soft matrix-GF composite materials, T_c, as a function of the tearing energy of the soft matrices, T_m. In this scaling plot, two series of polyampholyte (PA) tough hydrogels at different conditions, polyacrylamide (PAAm) weak hydrogels at different conditions, and a commercially available polydimethylsiloxane (PDMS) elastomer are utilized as soft matrices in the composites. In detail, in one series utilizing the PA hydrogel matrix (black circles, "PA (velocity series)"), the hydrogel toughness was tuned by changing the tearing velocity ranging from 1 to 1000 mm min^{-1}, based on the strong viscoelasticity of PA gels. In the other series of the PA hydrogel matrix (red circles, "PA (NaCl saline series)"), the hydrogel toughness was tuned using saline solutions with different salt concentrations (0–0.15 M), because the ionic complex in the PA gel network is sensitive to external salt ions. The open red circle represents the result of the as-prepared sample (salt concentration: 2.5 M). In the PAAm weak hydrogel matrix series (blue diamonds, "PAAm (as-prepared)"), the modulus and strength of the hydrogel were tuned by adjusting the chemical cross-linker percentage, yet the hydrogel toughness showed a slight change (see details in Figures S12 and S13, Supporting Information). Meanwhile, the as-prepared PAAm hydrogel was also deswollen in 20 wt% poly(ethylene glycol) (PEG, $M_w = 20000$) solution (purple diamond, "PAAm (PEG solution)") to achieve a similar deswelling behavior as the as-prepared PA hydrogel in deionized water, leading to slightly enhanced mechanical properties and toughness (see details in Figures S14 and S15, Supporting Information). A PDMS elastomer (green squares, "PDMS") with a moderate tearing energy (≈960 J m^{-2}) was also selected as a matrix (see details in Figures S16 and S17, Supporting Information). The width of all composite samples for the tearing test is $w = 45$ mm. The solid line represents a regression of the plotted data. The gray zone represents the expected tearing energy from an additive combination of the components, where T_f varies from 6 to 19 kJ m^{-2}.

of the two components, $T_c = T_m + T_f$. With increasing matrix toughness, the synergetic effect appears to show the relationship, $T_c \gg T_m + T_f$, and the toughness of the composite depends specifically on the toughness of the matrix, following the observed power-law relationship. These results likely suggest a more general relationship, $T_c = 220\ T_m^{0.64} + T_f$, for the given fabric system. This equation clearly demonstrates why previous attempts to create FRSCs with weak hydrogels ($T_f >> T_m$) were unsuccessful. High matrix toughness is required to achieve the synergistic toughening necessary to create extremely tough FRSCs. Understanding what determines the prefactor and the exponent of the power-law relation will help to predict the conditions required for the occurrence of the synergetic

effect of the composite. We consider that the geometry of the woven fabric, such as the weave size, weave density, and the weave pattern, will likely influence these factors. For example, when the sample width decreases, less bulk deformation can occur, and the synergetic effect might be weakened. In contrast, when the sample width increases, the composite failure is also accompanied by fiber breaking instead of pull-out alone, and as a result the matrix toughness effect should be maximized. These changes in the fracture mechanism should influence the scaling relationship. A more systematic study on the transition in fracture mechanism is ongoing. Understanding these parameters will allow for optimization of fiber reinforced soft composites.

4. Conclusions

In this work, the highly energy-dissipative PA hydrogel matrix has been proven to play a critical role in achieving extremely tough fabric reinforced hydrogel (PA-GF) composites that far exceed what could be expected from simply mixing the neat components. To universally explore the relationship between matrix toughness and composite toughness in FRSCs, a series of matrices, including weak polyacrylamide hydrogels and a commercially available polydimethylsiloxane elastomer, were further selected as soft matrices to create soft composites. The results demonstrate that for a given fabric geometry, the composite toughness is correlated to the matrix toughness, following an empirical power-law equation, $T_c = 220\ T_m^{0.64}$, over two orders of magnitude. This relationship is associated with the energy dissipation of the soft matrix phase by the deformation and fracture of the matrix during fiber pull-out. By selecting soft matrix materials that can dissipate large amounts of energy and possess optimized interfacial bonding, strong synergetic effects can be achieved, and one can develop composites with toughness far beyond what would be achieved by the simple additive rule of mixtures. The results match the synergistic increase in mechanical properties seen in tough biological materials. This work provides a good guide toward the design of FRSCs with extraordinary fracture resistance capacity.

5. Experimental Section

Materials: Plain weave glass fiber fabric (denoted as GF, surface density $\sigma_s = 590$ g m^{-2}, thickness $t = 0.59$ mm, single fiber diameter $\Phi = 14$ µm) composed of E-glass was purchased from Marukatsu Co., Ltd., Japan. The GF was used as received. Images of the GF are presented in Figure 1. The contact angle of water (droplet size 2.0 µL) of one glass fiber bundle was determined using a contact angle meter (Drop Master 300, Kyowa Interface Science Co. Ltd., Japan). High wettability of the glass fiber to water was observed, which ensured the good penetration of the precursor monomer solution into the fiber bundles by capillary force (Figure S2, Supporting Information).

DMAEA-Q (79 wt%, cationic monomer) was supplied by MT Aqua Polymer, Inc., Japan. NaSS, (anionic monomer), acrylamide (AAm, neutral monomer), *N*,*N*′-methylene-bis-acrylamide (MBAA, chemical cross-linker), and α-ketoglutaric acid (α-keto, photoinitiator) were purchased from Wako Pure Chemical Industries, Ltd., Japan. The chemical structures of all monomers are shown in Figure S1 (Supporting Information). All reagents were used as received, and Milli-Q (18.3 MΩ) water was used in all experiments.

Fabrication of PA-GF Hydrogel Composites: PA-GF hydrogel composites were fabricated via a facile in situ radical polymerization. Typically, for preparing PA-GF hydrogel composites, a sheet-like woven glass fiber fabric was embedded into a reaction cell consisting of a pair of glass plates divided by two silicone spacers, and the fabric sheet was sandwiched between the two spacers. Our previous study has revealed that the mechanical properties and tear resistance capacities of the hydrogel composites involved in this work are much larger than the neat hydrogel matrices,[34] indicating that the neat hydrogel past the limit of the thickness of the fabric on both sides of the sheet-like hydrogel composites plays a negligible role in the mechanical properties. Tests were performed to verify this behavior (Figure S3, Supporting Information), and consequently 0.5 mm silicon spacers were chosen for fabrication, resulting in an as-prepared sample thickness of ≈1.5 mm.

After that, the initial solution containing anionic monomer (NaSS), cationic monomer (DMAEA-Q), cross-linker (MBAA), and photoinitiator (α-keto) was prepared according to the previous studies.[18,30,31] Here, the total ionic monomer concentration and the molar fraction of anionic monomer were fixed at 2.5 M and 0.52, respectively, and the molar fractions of both cross-linker and initiator were 0.10 mol%, relative to the total monomer concentration. The precursor solution was injected into the above reaction cell under an argon atmosphere, followed by irradiation with 365 nm ultraviolet lamp for 11 h at ambient temperature to complete the polymerization. After polymerization, the as-prepared hydrogel composites were obtained, and then immersed in abundant deionized water for at least 5 d to remove residual chemicals until the deswelling equilibrium was reached. During this process, mobile counterions were dialyzed gradually, and the oppositely charged ions on the polymer chains formed dynamic ionic bonds through electrostatic attraction, and the interfacial bonding between the polyampholyte and glass fabric was also enhanced accordingly. Neat polyampholyte hydrogels were also synthesized by this procedure, without the fabric sheet embedded.

For studying the effect of ionic strength, both the H_2O-equilibrated neat gel and composites were transferred into different concentration NaCl solutions for 48 h to reach a new swelling equilibrium, before using for mechanical testing.

Fabrication of PAAm-GF Hydrogel Composites: PAAm-GF hydrogel composites were also prepared via an in situ radical polymerization. First, the glass fiber fabric was introduced into the reaction cell through the same method as in the fabrication of PA-GF gel composites. Then, the precursor solution containing neutral monomer (AAm), chemical cross-linker (MBAA), and photoinitiator (α-keto) was prepared. The monomer concentration was 2.5 M, and the concentrations of chemical cross-linker and photoinitiator were 0.1 mol% (or 5.0 mol%) and 0.1 mol%, respectively, relative to the monomer concentration. After that, the precursor solution was injected into the reaction cell, and the reaction conditions were the same as those of the PA-GF gel composites. The as-prepared PAAm-GF hydrogel composites were utilized for the tearing test. Neat polyacrylamide hydrogels were also prepared by the same procedure, without the embedded fabric sheet, and the hydrogels were also used in the as-prepared condition. To reduce the water content, the as-prepared samples were immersed in 20 wt% PEG ($M_w = 20\,000$) solution for 48 h. The sample thickness reduced from ≈1.47 mm to ≈1.05 mm by the high osmotic pressure of the polymer solution.

Fabrication of PDMS-GF Elastomer Composite: PDMS-GF composites were prepared by combining a commercially available PDMS (Dow Corning Toray Co., Japan) and woven glass fiber fabric. The weight ratio of the precursor of PDMS (SILPOT 184) to the cross-linker (CATALYST SILPOT 184) is 10:1, and the PDMS elastomer and PDMS-GF composites were cured in the reaction cell described above at 70 °C for 4 h.

Tearing Test: The tearing energy of the samples was evaluated by a typical trouser tearing test.[17,18,34,44] In Figure S19 (Supporting Information), the geometry of the trouser-shaped samples is sketched. A commercial tensile tester (Tensilon RTC-1150A, Orientec Co., Japan) equipped with a 1 kN load cell was used for the tearing test. The initial

notch (≈20 mm) was placed nominally in the center of the sample with a rotary cutter. For neat hydrogel samples, to prevent elongation of the legs of the sample during the test, stiff and thin tapes were glued on both sides of the samples prior to the test, as described elsewhere in the literature.[17] For hydrogel composite samples, to guarantee pull-out of the transverse fiber bundles, the length required to break, L_{bulk}, of the hydrogel was 5 mm larger than the width of one leg, $w/2$. During the test, one leg was clamped to the base, and the other leg was clamped to the crosshead, which was displaced at a constant velocity 50 mm min^{-1} (except for the study of the tearing velocity-dependence section) to tear the sample and obtain the tearing force–displacement (F–L) curve. A humidifier was used to supply a humid environment to minimize water evaporation in the hydrogel samples during the test. To evaluate the crack resistance capacity, the effective tearing energy, T, was calculated by integrating under a F–L curve to determine the energy required to break the samples, and divided by the projected area of new surface created, the thickness, t, multiplied by L_{bulk}:

$$T = \frac{\int_0^L F\,dL}{t \times L_{bulk}} \quad (1)$$

This method was described in detail in the previous study.[34] For the hydrogel composites, while the projected area, represented by t^*L_{bulk} or the area of the direct crack zone, does not include all of the new area made during tearing (which would include, for example, the additional area created by the friction process between fiber and gel), the resulting effective tearing energy closely matches that of Rivlin and Thomas, based on average tearing force, $\overline{F}$ ($T \approx 2\overline{F}/t$).[44] This approximation is therefore used to provide an easy calculation of tearing energy. Although the composite sample thickness varied with the formulation of the gels (1.47–3.35 mm at the as-prepared state), because the tearing force for the composite sample tested here is much larger compared to the neat gel in the same condition, the fabric thickness, t, was used to calculate the tearing energy of the composite samples. At least three tests were carried out for each sample, and the average value was calculated and the standard derivation was obtained as the error bar.

Tensile Test: The tensile test for the neat hydrogel samples was carried out by using a commercial tensile tester (Tensilon RTC-1310A, Orientec Co., Japan) equipped with a 100 N load cell at a crosshead velocity of 100 mm min^{-1} (except for the study of the tensile velocity-dependence section) in air. Before the test, the hydrogel samples were cut into a dumbbell shape standardized as JIS-K6251-7 (2 mm in inner width, 12 mm in gauge length) with a gel-cutting machine (Dumb Bell Co., Ltd.), as described in Figure S20 (Supporting Information). The sample thickness was 1–2 mm. During the test, a humidifier was used to supply a humid environment to minimize water evaporation of the hydrogel samples. At least three tests were carried out for each sample, and the average value was calculated and the standard derivation was obtained as the error bar.

Scanning Electron Microscopy: The surface morphologies of the neat fabric and the fractured composite samples were captured with a SEM (JEOL JSM-6010LA, Tokyo, Japan). For hydrogel samples, after the tearing test, the samples were dried at 60 °C in an oven for 2 d. Before observation, the samples were gold-coated in an ion-sputtering machine (E-1010, Hitachi, Tokyo, Japan). During the observation, the acceleration voltage varied from 10 to 20 kV.

Supporting Information

Supporting Information is available from the Wiley Online Library or from the author.

Acknowledgements

This research was supported by the Grant-in-Aid for Scientific Research (S) (No. 124225006) from the Japan Society for the Promotion of Science (JSPS). This research was also partially funded by the ImPACT Program of Council for Science, Technology and Innovation (Cabinet Office, Government of Japan). D.R.K. thanks the Hokkaido University Tenure Track System Promotion Program for partial funding. Y.H. thanks the MEXT, Japan for the scholarship during his PhD study. The authors also thank Prof. Alfred J. Crosby for fruitful discussions.

Received: October 14, 2016
Revised: November 10, 2016
Published online: January 13, 2017

[1] S. Lv, D. M. Dudek, Y. Cao, M. M. Balamurali, J. Gosline, H. Li, *Nature* **2010**, *465*, 69.
[2] R. O. Ritchie, *Nat. Mater.* **2011**, *10*, 817.
[3] U. G. K. Wegst, H. Bai, E. Saiz, A. P. Tomsia, R. O. Ritchie, *Nat. Mater.* **2015**, *14*, 23.
[4] Y. A. Shin, S. Yin, X. Li, S. Lee, S. Moon, J. Jeong, M. Kwon, S. J. Yoo, Y.-M. Kim, T. Zhang, H. Gao, S. H. Oh, *Nat. Commun.* **2016**, *7*, 10772.
[5] F. Barthelat, *Bioinspiration Biomimetics* **2010**, *5*, 35001.
[6] R. O. Ritchie, *Nat. Mater.* **2014**, *13*, 435.
[7] F. Libonati, G. X. Gu, Z. Qin, L. Vergani, M. J. Buehler, *Adv. Eng. Mater.* **2016**, *18*, 1354.
[8] K. Stok, A. Oloyede, *Clin. Biomech.* **2007**, *22*, 725.
[9] W. Yang, V. R. Sherman, B. Gludovatz, E. Schaible, P. Stewart, R. O. Ritchie, M. A. Meyers, *Nat. Commun.* **2015**, *6*, 6649.
[10] S. L.-Y. Woo, T. Q. Lee, S. D. Abramowitch, T. W. Gilber, in *Basic Orthopaedic Biomechanics & Mechano-Biology*, 3rd Ed., Lippincott Williams and Wilkins, Philadelphia, **2005**, pp. 301–342.
[11] W. J. Clegg, K. Kendall, N. M. Alford, T. W. Button, J. D. Birchall, *Nature* **1990**, *347*, 455.
[12] E. Munch, M. E. Launey, D. H. Alsem, E. Saiz, A. P. Tomsia, R. O. Ritchie, *Science* **2008**, *322*, 1516.
[13] M. D. Demetriou, M. E. Launey, G. Garrett, J. P. Schramm, D. C. Hofmann, W. L. Johnson, R. O. Ritchie, *Nat. Mater.* **2011**, *10*, 123.
[14] F. Bouville, E. Maire, S. Meille, B. Van de Moortèle, A. J. A. J. Stevenson, S. Deville, *Nat. Mater.* **2014**, *13*, 508.
[15] J. P. Gong, Y. Katsuyama, T. Kurokawa, Y. Osada, *Adv. Mater.* **2003**, *15*, 1155.
[16] J. P. Gong, *Soft Matter* **2010**, *6*, 2583.
[17] J.-Y. Sun, X. Zhao, W. R. K. Illeperuma, O. Chaudhuri, K. H. Oh, D. J. Mooney, J. J. Vlassak, Z. Suo, *Nature* **2012**, *489*, 133.
[18] T. L. Sun, T. Kurokawa, S. Kuroda, A. Bin Ihsan, T. Akasaki, K. Sato, M. A. Haque, T. Nakajima, J. P. Gong, *Nat. Mater.* **2013**, *12*, 932.
[19] F. Luo, T. L. Sun, T. Nakajima, T. Kurokawa, Y. Zhao, K. Sato, A. Bin Ihsan, X. Li, H. Guo, J. P. Gong, *Adv. Mater.* **2015**, *27*, 2722.
[20] H. J. Zhang, T. L. Sun, A. K. Zhang, Y. Ikura, T. Nakajima, T. Nonoyama, T. Kurokawa, O. Ito, H. Ishitobi, J. P. Gong, *Adv. Mater.* **2016**, *28*, 4884.
[21] M. P. E. Wenger, L. Bozec, M. A. Horton, P. Mesquida, *Biophys. J.* **2007**, *93*, 1255.
[22] S. Strasser, A. Zink, M. Janko, W. M. Heckl, S. Thalhammer, *Biochem. Biophys. Res. Commun.* **2007**, *354*, 27.
[23] A. J. Sophia Fox, A. Bedi, S. A. Rodeo, *Sport. Heal. A Multidiscip. Approach* **2009**, *1*, 461.
[24] F. T. Moutos, L. E. Freed, F. Guilak, *Nat. Mater.* **2007**, *6*, 162.
[25] A. Agrawal, N. Rahbar, P. D. Calvert, *Acta Biomater.* **2013**, *9*, 5313.
[26] I.-C. Liao, F. T. Moutos, B. T. Estes, X. Zhao, F. Guilak, *Adv. Funct. Mater.* **2013**, *23*, 5833.
[27] S. Lin, C. Cao, Q. Wang, M. Gonzalez, J. E. Dolbow, X. Zhao, *Soft Matter* **2014**, *10*, 7519.
[28] W. R. K. Illeperuma, J.-Y. Sun, Z. Suo, J. J. Vlassak, *Extreme Mech. Lett.* **2014**, *1*, 90.

[29] J. Visser, F. P. W. Melchels, J. E. Jeon, E. M. van Bussel, L. S. Kimpton, H. M. Byrne, W. J. A. Dhert, P. D. Dalton, D. W. Hutmacher, J. Malda, *Nat. Commun.* **2015**, *6*, 6933.
[30] A. Bin Ihsan, T. L. Sun, S. Kuroda, M. A. Haque, T. Kurokawa, T. Nakajima, J. P. Gong, *J. Mater. Chem. B* **2013**, *1*, 4555.
[31] C. K. Roy, H. L. Guo, T. L. Sun, A. Bin Ihsan, T. Kurokawa, M. Takahata, T. Nonoyama, T. Nakajima, J. P. Gong, *Adv. Mater.* **2015**, *27*, 7344.
[32] S. Rose, A. Prevoteau, P. Elzière, D. Hourdet, A. Marcellan, L. Leibler, *Nature* **2014**, *505*, 382.
[33] H. Yuk, T. Zhang, S. Lin, G. A. Parada, X. Zhao, *Nat. Mater.* **2015**, *15*, 190.
[34] D. R. King, T. L. Sun, Y. Huang, T. Kurokawa, T. Nonoyama, A. J. Crosby, J. P. Gong, *Mater. Horiz.* **2015**, *2*, 584.
[35] V. Gun'ko, V. Zarko, V. Turov, R. Leboda, E. Chibowski, E. Pakhlov, E. Goncharuk, M. Marciniak, E. Voronin, A. Chuiko, *J. Colloid Interface Sci.* **1999**, *220*, 302.
[36] H. Abe, Y. Hara, S. Maeda, S. Hashimoto, *J. Phys. Chem. B* **2014**, *118*, 2518.
[37] J. Ahmed, T. Yamamoto, H. Guo, T. Kurokawa, T. Nonoyama, T. Nakajima, J. P. Gong, *Macromolecules* **2015**, *48*, 5394.
[38] F. Luo, T. L. Sun, T. Nakajima, T. Kurokawa, Y. Zhao, A. Bin Ihsan, H. L. Guo, X. F. Li, J. P. Gong, *Macromolecules* **2014**, *47*, 6037.
[39] M. Rubinstein, R. H. Colby, *Polymer Physics*, Oxford University Press, New York **2003**.
[40] P. G. de Gennes, *Langmuir* **1996**, *12*, 4497.
[41] G. J. Lake, A. G. Thomas, *Proc. R. Soc. London, Ser. A* **1967**, *300*, 108.
[42] M. W. Keller, S. R. White, N. R. Sottos, *Adv. Funct. Mater.* **2007**, *17*, 2399.
[43] M. D. Bartlett, A. B. Croll, D. R. King, B. M. Paret, D. J. Irschick, A. J. Crosby, *Adv. Mater.* **2012**, *24*, 1078.
[44] R. S. Rivlin, A. G. Thomas, *J. Polym. Sci.* **1953**, *10*, 291.